Electrical conductivities for hot, dense hydrogen

I. Kwon,* L. Collins, and J. Kress
Theoretical Division, Los Alamos National Laboratory, Los Alamos, New Mexico 87545

N. Troullier
IBM-STSS Almaden Research Center, San Jose, California 95120
(Received 6 May 1996)

We report electrical conductivities for a hydrogen plasma at temperatures between a few tenths to a few tens of electron volts and densities ranging from 0.3 to 3 g/cm^3. The ac conductivities were determined within the Kubo-Greenwood formulation based on eigenstates from a finite-temperature density functional calculation at selected time steps along a lengthy molecular-dynamics (MD) simulation trajectory. Density functional, tight-binding, and effective pair potentials were employed in the MD simulations for samples of 50 to 250 atoms within a periodically replicated reference cell. We compare with other techniques and discuss trends with density and temperature. Good agreement results at the higher temperatures and densities with generalized Ziman forms. [S1063-651X(96)06109-0]

PACS number(s): 52.25.−b, 61.20.Ja, 05.60.+w

I. INTRODUCTION

Electrical conductivities play a vital role in the modeling of dense plasmas and have engaged the interest of theoreticians and experimentalists alike for many decades [1–4]. They have received renewed interest owing to recent shock experiments [5], showing large changes over small pressure regimes, and to theoretical predictions of plasma phase transitions [6,7], and of new facets in the equations of state [8–11]. Most of the current attention has centered at moderate to high densities and fairly low temperatures.

A variety of models have arisen to treat electrical conductivities of dense plasmas. One of the earliest invoked a two-component plasma (TCP) scheme [12] with a classical treatment of the electrons and ions. Many TCP thermodynamical properties have simple forms in terms of various plasma coupling coefficients, expressed as the ratio of the Coulombic to the kinetic energy. For example, in terms of the temperature T and number density of the ions n_i, the ion coupling coefficient Γ has the form $Ze^2/(r_s k_B T)$ with the dimensionless ion sphere radius parameter r_s given by a_s/a_B, where $a_s=[3/(4\pi n_i)]^{1/3}$ and a_B, the Bohr radius. The Fermi temperature $[T_F=(\hbar^2/2m_e)(3\pi^2 n_e)^{2/3}]$, related to the electron number density n_e and mass m_e, provides another useful descriptive quantity. The ratio $\Theta=T/T_F$ demarcates the regime between quantal and classical treatments of the electrons.

Various improvements have since been instigated to include quantum-mechanical effects. Some concentrate on solving the basic kinetic equations [13,14], while others employ a density response formalism (ITMY) [15] or more elaborate integral equation forms [16]. In this same vein, another class of models focuses on Green's function formulations, based either on linear response [7] or memory function [17] approaches. Still other treatments have evolved from extensions of the Ziman formula, which strictly applies to degenerate, strongly coupled plasmas. These models treat a representative atom at various levels of sophistication from average atom [18] to elaborate density functional schemes [19,20]. More recent investigations have moved beyond a single site to treat a reference cell with a large number of fully interacting atoms, evolving in time. All the electrons in the reference cell receive an equal quantum mechanical treatment, and the full dynamics of both the electrons and ions enter. Both quantum Monte Carlo [6,21] and molecular-dynamics [22–24] versions have recently appeared. The above presentation has only briefly sketched the various methods since a detailed exposition of the historical development and various physical approaches appear in earlier references [24].

In this paper we employ a quantum molecular-dynamics (QMD) approach to determine the electrical conductivity in a hot, dense plasma. The technique has considerable versatility and has been applied already to modeling other aspects of this medium [24]. The approach accounts for a wide variety of dynamical processes such as ionization-recombination, dissociation-bonding, and detachment-attachment. In addition, the properties of alkali-metal liquids [25], the metallization of rare gas solids [26], the development of tight-binding models [27] for dense H, line broadening of impurity atoms in a H plasma [28], and isotopic hydrogenic mixtures [29] have all received treatment with the technique. We begin with a brief description of the QMD method and conductivity models in Sec. II and present results and discussion in Sec. III. All of our calculations lie in the strongly coupled ($\Gamma \geqslant 1$) and electronically degenerate ($\Theta \leqslant 1$) regimes. In addition, we concentrate on an intermediate range of densities (0.3–3 g/cm^3) and temperatures (0.5–13.6 eV) that connect the fully classical to the fully quantum-mechanical regions. These complement the calculations of the Jülich group [23] at generally lower temperatures.

II. FORMALISM

For our applications, we apply a quantum molecular-dynamics approach to simulate the conditions within a dense

*Present address: Center for Theoretical Physics, Seoul National University, Seoul, 151-742, South Korea.

hydrogen plasma and the standard Kubo-Greenwood formulation to extract the electrical conductivity. Since the QMD techniques have received extensive treatment elsewhere [24], we briefly summarize the salient features of the method and focus on conductivity.

A. Simulations

The basic unit of the molecular-dynamics simulation consists of a cubic cell of length L containing equal numbers of electrons and protons ($n_e = n_p = N$). A periodic replication of this cell throughout space represents the fluid nature of the plasma. We invoke the Born-Oppenheimer approximation in which the nuclear and electronic motions separate and treat the speedy electrons quantum mechanically and the sluggish nuclei classically. In this case, a simple two-step procedure suffices to evolve the system in time. First, at a given time step for a fixed configuration of the nuclei, we solve the n_e-electron Schrödinger equation for the quantum mechanical force $\boldsymbol{F}_\alpha$ on each ion. Second, the ions are advanced temporally by solving the classical equations of motion

$$m_\alpha \ddot{\mathbf{r}}_\alpha = \boldsymbol{F}_\alpha , \tag{1}$$

where m_α is the mass of the αth nuclei and $\ddot{\mathbf{r}}_\alpha$ is its acceleration. Repeating the two-step process, we evolve the system in time by determining positions, velocities, forces, and electronic properties at each step.

1. Electronic structure

The first step of the simulation involves a calculation of the quantum-mechanical force on the ions. We instigate this calculation by solving the Schrödinger equation for n_e electrons and n_p fixed ions within a periodically replicated reference cell, relying upon both density-functional (DF) and tight-binding (TB) methods.

The finite-temperature density-functional procedure [31,32] provides the most accurate determination of the forces. Minimizing the Mermin functional $\Omega[\psi_i]$ with respect to variations of the density leads to a set of equations for the electron orbitals of the Kohn-Sham form

$$[-\tfrac{1}{2}\nabla^2 + V_{\mathrm{EXT}}(\mathbf{r}) + V_H(\mathbf{r}) + V_{\mathrm{XC}}(\mathbf{r})]\psi_i(\mathbf{r}) = \epsilon_i \psi_i(\mathbf{r}), \tag{2}$$

where V_H is the Hartree term, V_{XC} is the exchange-correlation term, and V_{EXT} is the interaction with an external potential. All of these terms depend implicitly on the electron density with orbitals populated according to a Fermi-Dirac distribution at the electron temperature T_e. We operate within the local density approximation (LDA) with a free-electron gas form for the exchange contribution and the Perdew-Zunger parametrization [33], based on the Ceperley-Alder Monte Carlo calculations [34], for the correlation contribution. For hydrogen, the external field takes the simple form of an electron interacting with the bare nuclei ($\Sigma_\alpha |\mathbf{r} - \mathbf{R}_\alpha|^{-1}$). Solution of Eq. (2) yields the orbitals that determine the value of the functional Ω, from which the forces on the ions arise from direct application of the spatial gradient. In determining the forces, we generally assume local thermodynamic equilibrium (LTE) with the electron and ion temperatures equal ($T_e = T_i$).

We solve the Kohn-Sham (KS) equations by first splitting the one-electron orbital ψ_i into a product of a simple plane wave in $\boldsymbol{k}$ and of a function periodic with respect to the image cells. We further expand this cell-periodic function in a plane-wave basis in terms of the reciprocal lattice vector $\boldsymbol{G}$. A matrix representation of the KS equations for a given $\boldsymbol{k}$ vector comes from multiplying the left side of Eq. (2) by a representative orbital and integrating over all spatial coordinates. We truncate the plane-wave expansion at a finite cutoff value $E_{\mathrm{cut}} (= \frac{1}{2}|\boldsymbol{G}_{\mathrm{cut}}|^2)$ and successively increase $\boldsymbol{G}_{\mathrm{cut}}$ until convergence in certain properties is attained. The truncation of the plane-wave expansion produces a matrix of finite size, which we diagonalize by iterative techniques [24] to produce a set of n_s eigenstates.

Even for hydrogen, the accurate treatment of the cusp condition at the nuclei necessitates the use of very large basis sets. To reduce the size of the basis, we have employed the Troullier-Martins pseudopotential [35] extended to nonlocal form by the Kleinman-Bylander prescription [36]. Using a small cutoff radius (r_c), typically of the order of r_s, affects only slightly the basic properties while significantly reducing the number of plane waves needed for convergence.

While the DF-LDA method described above allows a sophisticated treatment of the basic electron and ion interactions, the computational time necessary to evolve long trajectories for large samples of atoms becomes prohibitive. Therefore, we have developed a semiempirical potential based on a TB prescription [37,38]. In order to produce an effective model of the hydrogenic medium, we must construct a suitable representation of the TB matrix elements. We begin with a two-function basis on each atomic site consisting of s and s' orbitals. Fits to diatomic and bulk properties produce the desired functional forms for these matrix elements. The details of the construction and table of parameters for our hydrogenic TB ss' potential appear elsewhere [27]. Diagonalization of the TB matrix determines the electron orbitals. These orbitals in turn yield the total energy, whose spatial derivative gives the force acting upon an ion. We introduce temperature effects by populating the orbitals according to a Fermi-Dirac distribution at the ion temperature T_i. We also model the dense media by a simple Moliere pair potential [39], based on the Thomas-Fermi electronic screening function. Since the TB ss' contains no p-wave contribution and the Moliere has no electronic component at all, these two methods only apply for producing the dynamical configurations of the ions. Neither can directly produce electrical conductivities.

2. Molecular dynamics

All of our simulations employ constant density and volume. In order to preserve constant density within the cell, we also apply periodic boundary conditions in which a particle exiting the cell through one side is replaced by one entering on the opposite side. We consider both microcanonical and isokinetic ensembles. For the isokinetic ensemble, we fix the temperature at a prescribed value T_i and maintain this balance through a simple velocity scaling of the ratio of T_i to the average kinetic temperature T_K. We start the sample in a high symmetry state such as body-center cubic (bcc) and associate with each nucleus a random velocity consistent with a Maxwell-Boltzmann distribution at T_i. Successive

application of the velocity Verlet algorithm evolves the system in time. The resulting collection of positions and velocities of the nuclei at each time step defines a trajectory. In turn, Green-Kubo formulas, based on autocorrelation functions, relate the trajectory information to microscopic properties of the system such as diffusion and viscosity. In addition, the pair correlation function $g(r)$, which gives the probability of finding a particle at a distance r from a reference particle [30], provides another useful quantity that provides information on the nature of the fluid. Finally, since the nuclei move according to the classical equations of motion, we consider temperatures well above the regime in which the zero-point motion ($\sim$ 0.25 eV) becomes important.

B. Conductivities

The frequency-dependent electrical conductivity derived from the Kubo-Greenwood formulation [37,38] has the form (in a.u.)

$$\sigma(\omega)=C\sum_{ij} F[\epsilon_i,\epsilon_j]|D_{ij}|^2\delta(\epsilon_i-\epsilon_j-\omega), \tag{3}$$

where $C=2\pi/\Omega$ with Ω the atomic volume, and ω is the frequency. The other quantities include (1) the difference between the Fermi-Dirac distributions f_0 at a temperature T,

$$F[\epsilon_i,\epsilon_j]=[f_0(\epsilon_i)-f_0(\epsilon_j)]/\omega, \tag{4}$$

and (2) the velocity dipole matrix element,

$$|D_{ij}|^2=\frac{1}{3}\sum_{\alpha} |\langle\psi_i|\nabla_\alpha|\psi_j\rangle|^2. \tag{5}$$

Even though the system is assumed isotropic, the sum (α) extends over x,y, and z in order to improve the statistics. The quantities ϵ_i and ψ_i represent the energy and wave functions for the ith KS orbital found from the diagonalization of Eq. (2). The summation in i runs over all occupied states while that in j covers only unoccupied states. An analogous integral expression follows from the properties of the product δ function as

$$\sigma(\omega)=c\int F[E',E]|D(E'|E)|^2N(E')N(E)dE, \tag{6}$$

where the density of states per unit energy per unit volume,

$$N(E)=\Omega^{-1}\sum_i \delta(E-\epsilon_i), \tag{7}$$

$c=C\Omega^2$, $E'=E+\omega$, and $D(E'|E)$ is the analogue of Eq. (5) for a continuous range of energies. The integral spans all occupied orbitals, in other words, up to the Fermi energy ϵ_F. Finally, we define the dc conductivity as $\sigma_{\rm dc}=\sigma(0)$.

We evaluate the integral in Eq. (6) by partitioning into energy bins of equal size ΔE and determining averaged quantities within each bin from the discrete eigenstate calculations. Since the δ function causes $\sigma(\omega)$ to peak around ω, we can use Eq. (3) directly [23] and define an average conductivity as

$$\sigma_{\rm ave}(\omega)=\frac{1}{d\omega}\int_{\omega-d\omega/2}^{\omega+d\omega/2}\sigma(\omega')d\omega'. \tag{8}$$

Substituting Eq. (3) into Eq. (8) eliminates the δ function and yields a simple sum over the Fermi-Dirac distributions and the dipole matrix elements. The two approaches give results in excellent agreement for regimes relatively insensitive to the choice of ΔE and $d\omega$, respectively. The production of only a finite number of eigenstates places a restriction on the frequency range. We can obtain converged values of $\sigma(\omega)$ only for $\omega\leqslant|\epsilon_{n_s}-\epsilon_F|$ since larger values of ω connect to unoccupied excited states ϵ_i with $i\geqslant n_s$.

III. RESULTS AND DISCUSSION

Having completed a summary of the basic procedures employed to determine the electronic structure, the molecular-dynamics simulations, and the electrical conductivities, we embark upon a detailed description of a hot, dense hydrogen plasma. Before launching into the conductivity results, we first present an analysis of the accuracy of the underlying simulations.

A. Preliminaries

Since we employ parameters for these MD simulations similar to those in a earlier study [24], we simply summarize the salient findings. The DF-LDA calculations employed a pseudopotential with r_c equal to 1 bohr for $r_s=1$ and of 1.4 bohr for $r_s=1.4$, 2, and 2.5. This choice, even for the highest density treated, gave total energies within 10 mRy/atom of the exact $1/r$ pseudopotential results. In order to assure similar accuracies in the forces, we take a plane-wave truncation $E_{\rm cut}$ of 36(70) Ry for $r_s=1.4(1.0)$. The MD simulations generally use a time step (Δt) of 10–20 a.u. and a trajectory length of the order of ps. This range of step size guarantees the proper following of the fluctuations of various thermodynamical properties, such as the total energy in the isokinetic case, with between 15 and 20 time points within a wavelength. The energy deviates by less than 1% over the entire simulation with any drift confined to this narrow range. Properties that depend on autocorrelation functions, such as the diffusion coefficient, have accuracies on the order of a few percent. Since the TB and Moliere approaches take far less computational time per step, we have run these simulations with much smaller time steps and longer trajectories, yielding properties converged to better than 1%. For a detailed analysis, we refer the reader to our earlier work [24]. We defer the discussion of the accuracy of the conductivity until the next section.

B. Electrical conductivity

We have performed calculations for electrical conductivities over a temperature range between 5×10^3 and 1.5×10^5 K (0.5–13.6 eV) and a density regime of $\frac{1}{3}$ to 3 g/cm^3 ($r_s=$ 1–2). We begin with a discussion of various schemes for calculating σ as well as tests of accuracy, then describe the general results, and conclude with a comparison to other methods.

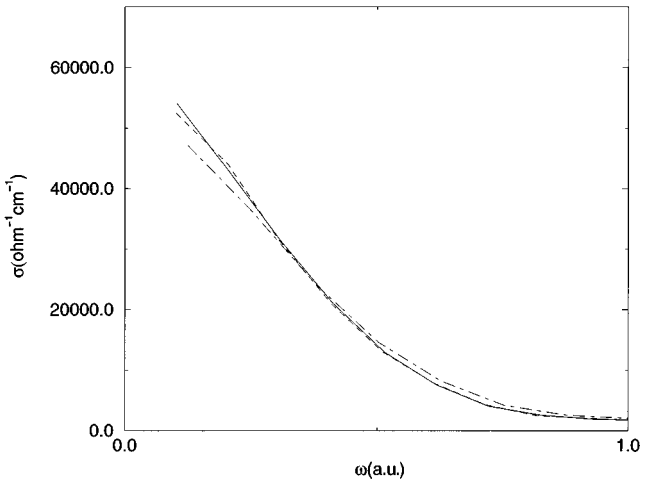

FIG. 1. Comparison of electrical conductivity as a function of frequency for various simulation-structure models for H at $r_s=1$ and $\Gamma=10$ for a sample of 108 atoms. PP-DF (solid line), TB-DF (dashed line), and DF-DF (dot-dashed line).

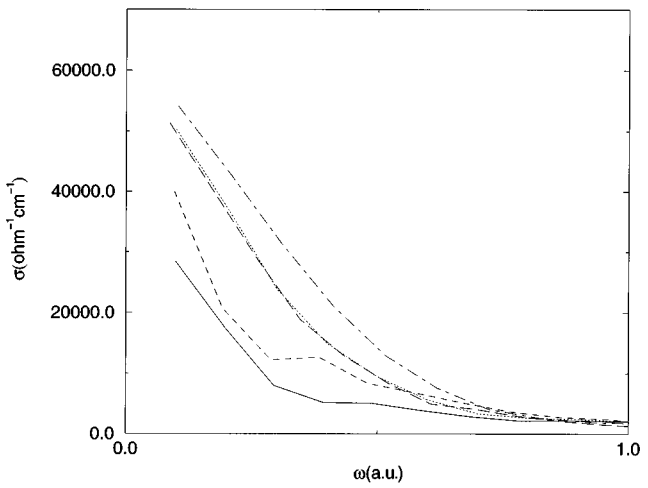

FIG. 2. Electrical conductivity as a function of frequency for $r_s=1$ and $\Gamma=10$ for different numbers of atoms (N) ($N=54$–250) in the reference cell. All cases employed the PP-DF model. Legend: $N = 54$ (solid line), 64 (short-dashed line), 108 (dot-dashed line), 128 (dotted line), and 250 (long-dashed line).

1. Simulation schemes and tests

The basic calculation of the electrical conductivity proceeds along the following lines. First, we generate a trajectory containing the positions of the particles for a collection of time steps n_t. Second, for a selected subset of times (snapshots), we perform a DF-LDA electronic structure calculation for the particle configurations and, from the KS orbitals and energies, we then generate the conductivity according to Eqs. (6) or (8). Third, the final electrical conductivity becomes an average over this temporal subset. Once the diffusion regime has been established, we usually take between 10 and 40 snapshots in the conductivity average with the snapshots separated by at least the correlation time (1/e falloff in the velocity autocorrelation function). We designate the various schemes for calculating $\sigma(\omega)$ as XX-YY where XX refers to the MD simulation technique [density functional, tight-binding, or Moliere pair potential (PP)], and YY to the electronic structure method employed in step 2, in all cases the density functional in the local density approximation. In addition, since we treat extended spatial systems, the DF-LDA calculations are generally confined to the Γ point [$\boldsymbol{k}=(2\pi/L)$ (0,0,0)]. We have found [24] that in certain temperature and density regimes the TB and PP provide very good quality trajectories as demonstrated by comparisons of dynamical and static properties with the more accurate DF-LDA results. Since these techniques consume far less computational time than the DF, they allow more stringent tests of size effects and trajectory parameters.

In order to gauge the efficacy of such mixed schemes, we present a representative example in Fig. 1 in which we compare the frequency-dependent conductivity for a density of 2.65 g/cm^3 ($r_s=1$) and a temperature of 2.72 eV ($\Gamma=10$) for three schemes: DF-DF, TB-DF, and PP-DF, with 108 atoms in a reference cell. The agreement remains good throughout the whole frequency range. At the lowest frequencies, the methods depart slightly with the DF-DF about 10% lower than the other two approaches. The very low frequencies sample a small region around the Fermi level, which depends more critically on the actual dynamics technique employed. We have observed similar behavior for a 64-atom sample. At lower densities, the pair potential gives less satisfactory results while the tight binding provides sound trajectories throughout the entire density-temperature regime studied.

One of the most important tests rests with the convergence of $\sigma(\omega)$ with the size of the sample. All the simulations employ a single-point k-space integration, which should become more accurate as the number of atoms in the reference cell increases. Since the density remains fixed, this also tests the sensitivity to the volume of the cell, L^3. In Fig. 2, we present a comparison of σ as a function of frequency for $r_s=1$ and $\Gamma = 10$ (2.65 g/cm^3; 2.72 eV) for 54, 64, 108, 128, and 250 atoms. The convergence goes slowly as a function of N until near the 100-atom level. This behavior stems from a large band gap in the eigenspectrum of the smaller samples for which finite temperature effects only barely compensate. For the larger samples, the gap narrows, giving rise to larger conductivities. This explanation also accounts for the kink in the $N=64$ results. At the lower frequencies, the agreement between the 108- and 250-atom cases is on the order of 15% and much better at higher frequencies. Such findings hold over our range of densities and temperatures.

Ideally, we would like to perform a full k-space integration for each choice of N and L. However, this at present remains outside the purview of our techniques and would be prohibitive within any lengthy DF-LDA simulation. Still, in addition to the test of cell size, we can also examine the sensitivity with respect to special k-space integration points, which also reflects size effects. In Fig. 3, we present a comparison between $\sigma(\omega)$ for an $N=108$ sample at $r_s=1$ and $\Gamma=5$ for integrations involving two distinct k points: $(2\pi/L)(0,0,0)$ and $(2\pi/L)(\frac{1}{4},\frac{1}{4},\frac{1}{4})$. The former represents the Γ and the latter the Baldereschi [40] point. We note a 15% difference at the lower frequencies. A consistent trend develops with the Baldereschi point result for 108 atoms moving in the direction of the 250-atom sample at the Γ point. Since most of the simulations employ a sample of 108 atoms, we

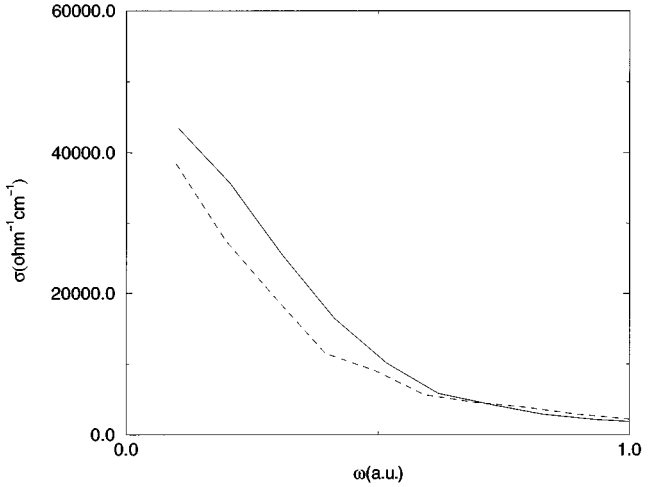

FIG. 3. Electrical conductivity as a function of frequency with $r_s=1$ and $\Gamma=5$ for different k-point integration schemes: Γ point (solid line) and Baldereschi point (dashed line) for $N=108$ in the PP-DF model.

would judge at these densities that sample size effects may account for an error on the order of 20%.

We have determined the dc conductivity by simple extrapolation schemes. Such extrapolation becomes necessary since the DF calculations produce ac conductivities only at finite frequencies. The lowest frequency obtainable corresponds to the smallest difference between the KS eigenenergies ϵ_i. These differences, in turn, are set by the sample size and the potential and dynamical models. We typically fit $\sigma(\omega)$ with a low-order polynomial (third to fifth order) by a standard least-squares technique and find $\sigma_{\rm dc}$ by an evaluation at $\omega=0$. Sensitivities to the type of fit generally remain at the few percent level. The departure of the DF-DF ac conductivities from the other two models at very low frequencies implies that the dc conductivity in the TB-DF or PP-DF may have additional error of approximately 15%. Therefore, the dc conductivities in these latter two models at $N=108$ may attain overall errors on the order of 25% . One final note is in order. For all our error analysis, we have employed the converged DF-DF model as the absolute. However, systematic errors due to nonlocal electronic density effects, for example, remain outside of our analysis since they would require more elaborate DF schemes. In addition, we have based the conductivity calculations on an excited manifold of quasiparticle states of the DF-LDA scheme. As long as the integration covers a reasonably dense DOS, then the approach produces reliable conductivities even though some ambiguity may attach to the physical interpretation of individual states.

2. MD results

We display in Fig. 4 and Table I a summary of our MD simulations for the electrical conductivity. In the table, we report dc conductivities found by extrapolating $\sigma(\omega)$ to zero frequency. All calculations employed a sample of 108 atoms and the TB-DF model for all cases with $r_s=1.4$ and 2 and the PP-DF for $r_s=1$. As mentioned above, we performed systematic checks of these two models with the DF-DF at selected values of n_i and T. One general feature readily

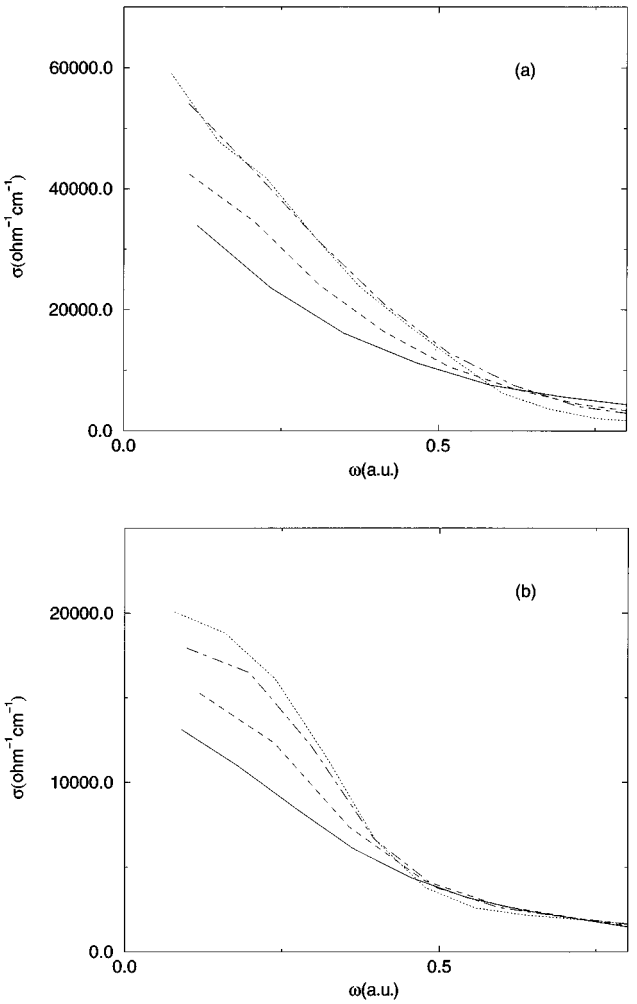

FIG. 4. Electrical conductivity as a function of frequency for two densities and various temperatures for $N=108$. Legend: (a) $r_s=1$ (PP-DF model) with $\Gamma=2$ (solid line), 5 (dashed line), 10 (dot-dashed line), and 20 (dotted line); (b) $r_s=1.4$ (TB-DF model) with $\Gamma=5$ (solid line), 10 (dashed line), 20 (dot-dashed line), and 40 (dotted line).

emerges from the results. Namely, for a given density (r_s), the conductivity decreases with increasing temperature—the general trend observed for a metal. In the most dense case (2.65 g/cm^3, $r_s=1$), the medium remains an atomic or completely dissociated fluid as seen from the plot of the pair-correlation functions in Fig. 5. At the lower density of 1 g/cm^3, the medium remains basically atomic until the lowest temperature, where vestiges of a molecular peak begin to appear as a kink around 1.4 a_B in the $g(r)$ of Fig. 6. The lowest density of 0.33 g/cm^3 retains also a purely atomic quality due to the high temperature. Finally, the conductivity does not behave as a simple function of plasma coupling constant as evidenced by the results for $\Gamma=10$ in Table I, where σ differs by an order of magnitude for three different temperature-density points.

3. Comparisons

We begin with a comparison to two simple formulas, the Spitzer and Mott. The Spitzer formula, which applies at high T and low density, goes off scale for our regime, which lies

TABLE I. H dc conductivities as a function of density and temperature. The brackets represent the power of 10. Model PP-DF for $r_s=1$ and TB-DF for $r_s = 1.4$, 2, and 2.5.

r_s	n (cm^{-3})	ρ ($\mathrm{g/cm}^3$)	Γ	T (K)	T (eV)	σ [$(\Omega\ \mathrm{cm})^{-1}$]
1.0	1.61(+24)	2.675	20	15780	1.36	6.65[+4]
			10	31580	2.72	6.30[+4]
			5	63160	5.44	5.00[+4]
			2	157900	13.61	4.25[+4]
1.4	6.02(+23)	1.000	40	5690	0.49	2.00[+4]
			20	11380	0.98	1.85[+4]
			10	22990	1.96	1.70[+4]
			5	45510	3.92	1.40[+4]
2.0	2.09(+23)	0.334	10	15780	1.36	3.50[+3]
2.5	1.00(+23)	0.166	8	15780	1.36	1.40[+3]

at the opposite extremes. The Mott formula [41] represents a simplification of the Kubo-Greenwood in Eq. (3) and relates the dc electrical conductivity to the density-of-states (DOS), $\mathscr{N}$, at the Fermi energy (ϵ_F) and to the average nearest-ion separation r_{NN}:

$$\sigma_{\mathrm{dc}}(\mathrm{Mott}) = 2.885\times 10^5 r_{NN}\mathscr{N}(\epsilon_F)^2, \tag{9}$$

with σ, r_{NN}, and $\mathscr{N}$ in units of $(\Omega\ \mathrm{cm})^{-1}$, bohr, and $(\mathrm{bohr}^3\ \mathrm{hartree})^{-1}$, respectively. The DOS comes from the DF-LDA calculation at each snapshot time step of the corresponding MD simulation. An average over the snapshot values produces the final value just as in the full Kubo-Greenwood case. Two basic approximations pertain: (1) the dipole matrix element becomes simply r_{NN}/Ω in the random-phase approximation, and (2) the DOS sharply peaks around ϵ_F. These approximations make this form of the Mott formula applicable mainly in the regime of high density and low temperature. In the case of liquid carbon [42], which behaves as a weak conductor, the Mott expression yields accurate conductivities. Our calculations, on the other hand, have centered in a regime in which hydrogen becomes a highly efficient conductor. For $r_s=1$, we find the Mott expression yields conductivities about a factor of 5–7 too low compared to the MD results for Γ between 5 and 20. For the lower density region ($r_s=1.4$), σ_{dc} (Mott) behaves only slightly better with the MD conductivities about four times higher ($5 \leqslant \Gamma \leqslant 40$). Therefore, in this case, the Mott form gives only an order-of-magnitude estimate of σ_{dc}.

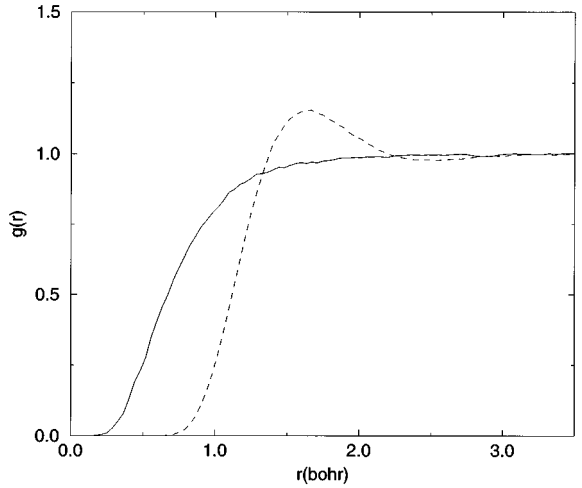

FIG. 5. Pair correlation functions for $r_s=1$ and $\Gamma = 2$ (solid line) and 20 (dashed line) in the PP-DF model.

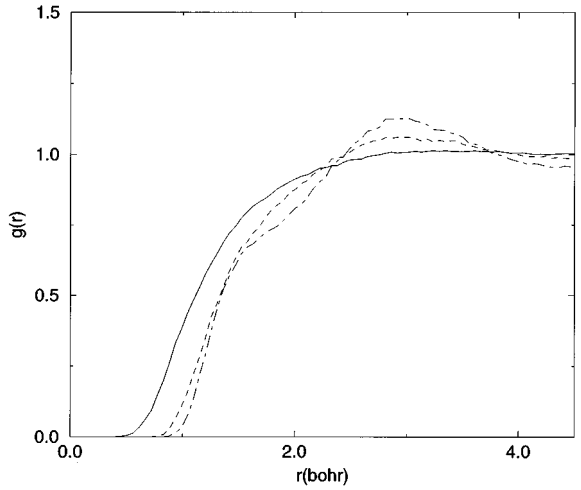

FIG. 6. Pair correlation functions for $r_s=1.4$ and $\Gamma = 5$ (solid line), 20 (dashed line), 40 (dot-dashed line) in the TB-DP model.

In Table II, we compare our MD simulations for the dc electrical conductivity with the thermodynamical Green's function approach of Berkovsky [17] and the generalized Ziman formulation within DF theory of Perrot and Dharmawardana [20]. The latter employs both the strong isolated (SIS) and the strong multiple (SMS) scattering forms. Only the MD results explicitly account for ionic fluctuations. For a high density (2.62 $\mathrm{g/cm}^3$) and temperature (2.72–13.6 eV), we obtain very good agreement with these other two approaches. In fact, the MD results lie bounded within the SIS and SMS over the whole range of T. The uncertainties in σ_{dc} prevent distinguishing between the two scattering models although a trend from SMS at low T to SIS at high T appears suggested. For dynamical simulation in this regime, we have shown [24] that fairly simple models such as effective pair potentials give, on average, a reasonable description of the

TABLE II. Comparison of H dc conductivities in units of $10^4\ \Omega^{-1}\ \mathrm{cm}^{-1}$ for $r_s=1$ and various values of Γ. MD refers to the present results, B to Ref. [17], PD to Ref. [20], TCP to Ref. [12], and ITMY to Ref. [15]. For the PD case, the first (second) entry refers to the SIS (SMS) model. For the TCP case, the first (second) entry refers to without (with) electron symmetry effects.

Γ	σ_{dc}				
	MD	B	PD	TCP	IMTY
10	6.3	6.3	5.1;6.2		
5	5.0	5.6	4.6;5.5		
2	4.3	5.0	4.3;4.9	9;12	12.4

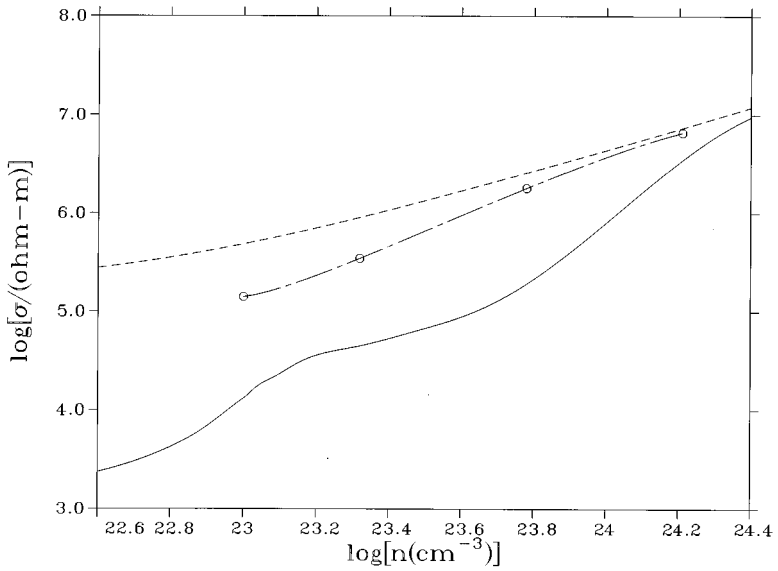

FIG. 7. dc electrical conductivity as a function of density at $T=15\,000$ K. The solid (dashed) line represents partially (fully) ionized H from Ref. [7]; circles represent present results for $N=108$ in the TB-DF model. Both axes are $\log_{10}$.

basic structure of the plasma as evidenced in the pair-correlation functions and diffusion coefficients. Therefore, we might expect that an atomic model perturbed, for example, by a hypernetted-chain representation of the structure would yield reasonable results. In an earlier study [24], we found evidence even at this elevated temperature of the transient formation of small molecular associations. A few percent of the atoms at any one time appeared engaged in such collections. This effect does not seem to influence the electrical conductivity, a property averaged over many states and configurations. At the highest temperature, we also compare with the classical two-component plasma model of Hansen and McDonald [12] and the ITMY model [15]. Even at this temperature, the degeneracy parameter Θ still lies well below unity (0.272), but in a range in which a classical treatment of the electrons might begin to pertain. For all the other temperatures, the value of Θ lies in a regime where quantum-mechanical effects become increasingly important.

In Fig. 7, we plot the dc conductivity as a function of density for a fixed temperature of 1.36 eV (15 870 K) and compare to the results of Reinholz, Redmer, and Nagel [7]. Their studies included both fully ionized (dashed line) and partially ionized (solid line) systems at $T=15\,000$ K. Since the conductivity from the TB-DF model exhibits little sensitivity to temperature between 10 000 and 20 000 K (Table I), we have extracted a value for $r_s=1.4$ by a simple interpolation. In the LDA simulations, the conductivity drops by nearly two orders of magnitude for r_s increasing from 1 to 2.5. This result lies closer to, though systematically below, the fully ionized case, being consistent with the large degree of dissociation we observe. All three models appear to merge at the higher densities. For the three most dense cases ($r_s=1$, 1.4, and 2), the frequency-dependent electrical conductivity rises as ω approaches zero. However, the behavior for $r_s=2.53$ changes, becoming almost flat for ω from 0.2 a.u. into the origin. This behavior closely resembles that of liquid carbon [42].

To summarize, we have presented a study of the behavior of the electrical conductivity as a function of density and temperature over an important regime for a hot, dense hydrogen plasma. We tested models of varying sophistication from density functional to simple pair potentials. The conductivities display general metallic properties of decreasing magnitude for increasing temperature at a fixed density.

ACKNOWLEDGMENTS

We gratefully acknowledge useful conversations with Dr. B. Holian and Dr. J. Erpenback. We wish to recognize many suggestions and contributions, especially in regard to the calculation of conductivities, offered by Dr. Oliver Pfaffenzeller and Professor Detlef Hohl of Jülich. We would also like to thank Professor Redmer for sending tables of their conductivities and helpful comments. This work was performed under the auspices of the U.S. Department of Energy through the Theoretical Division of the Los Alamos National Laboratory.

[1] H.K. Mao and R.J. Hemley, Rev. Mod. Phys. **66**, 671(1994).

[2] N.W. Ashcroft, Nature **340**, 345 (1989); *Molecular Systems Under High Pressure*, edited by R. Pucci and G. Piccito (Elsevier Science, Amsterdam, 1991); E. Kaxiras, J. Broughton, and R.J. Hemley, Phys. Rev. Lett. **67**, 1138 (1991), and references therein.

[3] *Strongly Coupled Plasmas*, edited by F.J. Rodgers and H.E. DeWitt (Plenum, New York, 1988); *Strongly Coupled Plasma*

Physics, edited by H.M. van Horn and S. Ichimaru (Rochester Press, Rochester, 1993).

[4] Special journal issues: J. Quant. Spectrosc. Radiat. Transfer **51**, No. 1/2 (1994); **54**, No. 1/2 (1995), special issues on radiative properties in hot dense matter, edited by R. W. Lee.

[5] S.T. Weir, A.C. Mitchell, and W.J. Nellis, Phys. Rev. Lett. **76**, 1860 (1995); W.J. Nellis, M. Ross, and N.C. Holmes, Science **269**, 1245 (1995).

[6] C. Pierleoni, D.M. Ceperley, B. Bernu, and W.R. Magro, Phys. Rev. Lett. **73**, 2145 (1994); V. Natoli, R. M. Martin, and D. M. Ceperley, Phys. Rev. Lett. **70**, 1992 (1993).

[7] H. Reinholz, R. Redmer, and S. Nagel, Phys. Rev. E **52**, 5368 (1995).

[8] A. Alavi, M. Parrinello, and D. Frenkel, Science **269**, 1252 (1995).

[9] J.I. Penman, J. Clérouin, and G. Zèrah, Phys. Rev. E **51**, R5224 (1995); J. Clérouin, E.L. Pollock, and G. Zèrah, Phys. Rev. A **46**, 5130 (1992).

[10] J. Kohanoff and J.P. Hansen, Phys. Rev. Lett. **74**, 626 (1995).

[11] D. Saumon, G. Chabrier, and H.M. Van Horn, Astrophys. J. Suppl. **99**, 713 (1995).

[12] J.P. Hansen and I.R. McDonald, Phys. Rev. A **23**, 2041 (1981); L. Sjogren, J.P. Hansen, and E.L. Pollock, Phys. Rev. A **24**, 1544 (1981).

[13] Y.T. Lee and R. More, Phys. Fluids **27**, 1273 (1984).

[14] D. Kremp, M. Schlanges, and K. Kilimann, Phys. Lett. **100A**, 149 (1984).

[15] S. Ichimaru and S. Tanaka, Phys. Rev. A **32**, 1790 (1985).

[16] S. Tanaka, X.-Z. Yan, and S. Ichimaru, Phys. Rev. A **41**, 5616 (1990); H. Kitamura and S. Ishimaru, Phys. Rev. E **51**, 6004 (1995).

[17] M.A. Berkovsky, Physica A **214**, 461 (1995).

[18] J.K. Yuan, Y.S. Sun, and S.T. Zhang, Phys. Rev. E **53**, 1059 (1996).

[19] G.A. Rinker, Phys. Rev. A **37**, 1284 (1988).

[20] F. Perrot and M.W.C. Dharma-wardana, Phys. Rev. A **36**, 238 (1987); Phys. Rev. E **52**, 5352 (1995).

[21] D.M. Ceperley and B.J. Alder, Phys. Rev. B **36**, 2092 (1987).

[22] D. Hohl, V. Natoli, D.M. Ceperley, R.M. Martin, Phys. Rev. Lett. **71**, 541 (1993); M.P. Grumbach, D. Hohl, R.M. Martin, and R. Car, J. Phys. Condens. Matter **6**, 1999 (1994).

[23] O. Pfaffenzeller, thesis IFF Jülich, 1996; O. Pfaffenzeller and D. Hohl (private communication).

[24] L. Collins, I. Kwon, J. Kress, and N. Troullier, Phys. Rev. E **52**, 6202 (1995); I. Kwon, L. Collins, J. Kress, N. Troullier, and D. Lynch, Phys. Rev. E **49**, R4771 (1994); L. Collins, J. Kress, I. Kwon, D. Lynch, and N. Troullier, in *Atomic Processes in Plasmas*, edited by W. L. Rowan, AIP Conf. Proc. 322 (AIP, New York, 1995), p. 187; L.A. Collins, J.D. Kress, D.L. Lynch, and N. Troullier, J. Quant. Spectrosc. Radiat. Transfer **51**, 65 (1994).

[25] D.L. Lynch, N. Troullier, J.D. Kress, and L. Collins, J. Chem. Phys. **101**, 7048 (1994).

[26] I. Kwon, L. Collins, J. Kress, and N. Troullier, Phys. Rev. B **52**, 15 165 (1995).

[27] I. Kwon, J. Kress, and L. Collins, Phys. Rev. B **50**, 9118 (1994).

[28] J. Kress, I. Kwon, and L. Collins, J. Quantum Spectrosc. Radiat. Transfer **54**, 237 (1995).

[29] I. Kwon, L. Collins, J. Kress, and N. Troullier, Europhys. Lett. **29**, 537 (1995).

[30] M. P. Allen and D. J. Tildesley, *Computer Simulation of Liquids* (Oxford Science, Oxford, 1987); J.M. Haile, *Molecular Dynamics Simulations* (Wiley, New York, 1992).

[31] N.D. Mermin, Phys. Rev. **137A**, 1441 (1965).

[32] R. Wentzcovitch, J.L. Martins, and P.B. Allen, Phys. Rev. B **45**, 11 372 (1992); R.M. Wentzcovitch and J.L. Martins, Solid State Commun. **78**, 831 (1991).

[33] J.P. Perdew and A. Zunger, Phys. Rev. B **23**, 5048 (1981).

[34] D.M. Ceperley and B.J. Alder, Phys. Rev. Lett. **45**, 566(1980).

[35] N. Troullier and J.L. Martins, Phys. Rev. B **43**, 1993 (1991).

[36] L. Kleinman and D.M. Bylander, Phys. Rev. Lett. **48**, 1425 (1982).

[37] W.A. Harrison, *Solid State Theory* (McGraw-Hill, New York, 1970).

[38] N.W. Ashcroft and N.D. Mermin, *Solid State Physics* (Saunders, Philadelphia, 1976).

[39] I.M. Torres, *Interatomic Potentials* (Academic, New York, 1972).

[40] A. Baldereschi, Phys. Rev. B **7**, 5212 (1973).

[41] N.F. Mott and E.A. Davis, *Electronic Processes in Non-Crystalline Materials* (Clarendon Press, Oxford, 1979).

[42] G. Galli, R.M. Martin, R. Car, and M. Parrinello, Phys. Rev. B **42**, 7470 (1990).